Structural Analysis of Nano Core PCF With Fused Cladding for Supercontinuum Generation in 6G Networks

Rajesh Anbazhagan, S. Chandru, Ravikumar Chinthaginjala, Kalapraveen Bagadi, Mohammad Alibakhshikenari, Bal Virdee, Syed Mansoor Ali, Iyad Dayoub, Patrizia Livreri, Sonia Aïssa

▶ **To cite this version:**

Rajesh Anbazhagan, S. Chandru, Ravikumar Chinthaginjala, Kalapraveen Bagadi, Mohammad Alibakhshikenari, et al.. Structural Analysis of Nano Core PCF With Fused Cladding for Supercontinuum Generation in 6G Networks. Radio Science, 2023, 58 (9), 10.1029/2023RS007690 . hal-04240654

HAL Id: hal-04240654
https://hal.science/hal-04240654

Submitted on 13 Oct 2023

HAL is a multi-disciplinary open access archive for the deposit and dissemination of scientific research documents, whether they are published or not. The documents may come from teaching and research institutions in France or abroad, or from public or private research centers.

L'archive ouverte pluridisciplinaire **HAL**, est destinée au dépôt et à la diffusion de documents scientifiques de niveau recherche, publiés ou non, émanant des établissements d'enseignement et de recherche français ou étrangers, des laboratoires publics ou privés.

Distributed under a Creative Commons Attribution 4.0 International License

Check for updates

AGU ADVANCING EARTH AND SPACE SCIENCES

Radio Science®

RESEARCH ARTICLE
10.1029/2023RS007690

Structural Analysis of Nano Core PCF With Fused Cladding for Supercontinuum Generation in 6G Networks

Rajesh Anbazhagan[1], S. Chandru[2], Ravikumar Chinthaginjala[3], Kalapraveen Bagadi[3], Mohammad Alibakhshikenari[4], Bal S. Virdee[5], Syed Mansoor Ali[6], Iyad Dayoub[7,8], Patrizia Livreri[9], and Sonia Aïssa[10]

[1]School of Electrical and Electronics Engineering, SASTRA Deemed University, Thanjavur, India, [2]Department of ECE, Global Institute of Engineering and Technology, Vellore, India, [3]School of Electronics Engineering, Vellore Institute of Technology, Vellore, India, [4]Department of Signal Theory and Communications, Universidad Carlos III de Madrid, Leganés, Spain, [5]Center for Communications Technology, School of Computing and Digital Media, London Metropolitan University, London, UK, [6]Department of Physics and Astronomy, College of Science, King Saud University, Riyadh, Saudi Arabia, [7]Université Polytechnique Hauts-de-France, Institut d'Électronique de Microélectronique et de Nanotechnologie (IEMN) CNRS UMR 8520, ISEN, Centrale Lille, University of Lille, Valenciennes, France, [8]INSA Hauts-de-France, Valenciennes, France, [9]Department of Engineering, University of Palermo, Palermo, Italy, [10]Institut National de la Recherche Scientifique (INRS), Université du Quebec, Montreal, QC, Canada

Abstract The Sixth Generation (6G) networks have identified the use of frequency range between 95 GHz and 3 THz with a targeted data rate of 1 Terabytes/second at the access network for holographic video applications. As is demands broadening of spectrum at the core network, this paper proposes a Supercontinuum Generation (SCG) through photonic crystal fiber (PCF) as it provides excellent broadening of the optical spectrum. Discussed in the paper is supercontinuum generation at high pumping power as per the standards specified by the International Telecommunications Union. The proposed PCF is designed with silicon nanocrystal core and the cladding microstructures is arranged in a fusion approach to effectively optimize the optical parameters such as dispersion, nonlinearity, birefringence, group-velocity dispersion, and confinement loss. The fused cladding comprises of a flower-cladding assembly in which air-holes arrangement is inspired from petals in a pleated structure. Such arrangement is shown here to provide high nonlinearity and negative dispersion for high power supercontinuum generation. The novel nanocore assembly with improved structural constraints delivers a non-linearity of 6.37×10^6 W^{-1} km^{-1} and a negative dispersion of −142.1 (ps/nm-km) at 1,550 nm. Moreover, a supercontinuum spectrum is generated using different pulse widths ranging from 350 to 650 ps with 25 kW pump power for PCF lengths of 10 and 15 mm.

Key Points:

- A Supercontinuum Generation through photonic crystal fiber (PCF) is proposed which provides excellent broadening of the optical spectrum
- PCF designed with silicon nanocrystal core and cladding microstructures is arranged in fusion approach to optimize the optical parameters
- The structural analysis of nano-core PCF with fused cladding provides a baseline for designing the 6G architecture

Correspondence to:
R. Chinthaginjala and M. Alibakhshikenari,
cvrkvit@gmail.com;
mohammad.alibakhshikenari@uc3m.es

Citation:
Anbazhagan, R., Chandru, S., Chinthaginjala, R., Bagadi, K., Alibakhshikenari, M., Virdee, B. S., et al. (2023). Structural analysis of nano core PCF with fused cladding for supercontinuum generation in 6G networks. *Radio Science*, *58*, e2023RS007690. https://doi.org/10.1029/2023RS007690

Received 27 FEB 2023
Accepted 9 AUG 2023
Corrected 3 OCT 2023

This article was corrected on 3 OCT 2023. See the end of the full text for details.

Author Contributions:
Conceptualization: Rajesh Anbazhagan, Bal S. Virdee
Data curation: Rajesh Anbazhagan, Kalapraveen Bagadi
Formal analysis: S. Chandru, Mohammad Alibakhshikenari, Sonia Aïssa
Funding acquisition: Mohammad Alibakhshikenari

© 2023. The Authors.
This is an open access article under the terms of the Creative Commons Attribution License, which permits use, distribution and reproduction in any medium, provided the original work is properly cited.

1. Introduction

The broadening of the spectrum for Sixth Generation (6G) networks can be realized in two different ways, namely, levitating the pump power in pre-amplification stage or varying the wavelength of pump to zero-dispersion wavelength. In many cohesive applications of Supercontinuum Generation (SCG), the most feasible and economical material is Silicon (Si). But, the disadvantage of using this material is that it has a high impact on two-photon absorption that constraints the broadening of the spectrum. Hence, materials which do not have any impact on nonlinear absorption have raised interest. The micro-structured fiber commonly known as Photonic Crystal Fiber (PCF) comprises numerous air-holes distributed periodically over the longitudinal axis has attracted attention due to its extraordinary features such as high nonlinear properties, optimizable dispersion, well-behaved mode area, and endlessly single-mode guidance (M. Abdullah-Al-Shafi & Sen, 2021; M. S. Hossain, et al., 2021; A. K. Vyas, 2021). PCF is broadly classified into two types based on the mechanism of the guidance of light propagated as effective-index guidance and photonic bandgap PCF (Y. Guo, et al., 2021; M. A. Islam, et al., 2021; Y. L. She, et al., 2021; Y. Qu, et al., 2021).

To exhibit high birefringent and non-linearity, a compressed PCF using hexagonal arrangement of circular holes has been discussed in (B. Yu & H. Rui, 2019). At a wavelength of 1,550 nm, the PCF structure display non-linearity of 42.58 W^{-1} $km^{-1}$and birefringence equal to 0.0159. Here, the core region of the PCF encompasses micro holes arranged in a definite pattern. The PCF is constructed using silica through perfectly matched layer (PML) setting. To improve the non-linearity, the holes have been coated using gold with silica background (A. Dixit, et al., 2017). Here, the construction of holes in outer cladding section is carried out as hexagonal

Investigation: Ravikumar Chinthaginjala, Kalapraveen Bagadi, Mohammad Alibakhshikenari, Bal S. Virdee
Methodology: S. Chandru, Syed Mansoor Ali, Iyad Dayoub, Patrizia Livreri
Project Administration: Ravikumar Chinthaginjala, Kalapraveen Bagadi, Mohammad Alibakhshikenari
Resources: Rajesh Anbazhagan, S. Chandru, Ravikumar Chinthaginjala, Patrizia Livreri
Software: Rajesh Anbazhagan, S. Chandru
Supervision: Ravikumar Chinthaginjala, Kalapraveen Bagadi, Mohammad Alibakhshikenari
Validation: Rajesh Anbazhagan, S. Chandru, Ravikumar Chinthaginjala, Kalapraveen Bagadi, Mohammad Alibakhshikenari, Bal S. Virdee, Syed Mansoor Ali, Patrizia Livreri, Sonia Aïssa
Visualization: Syed Mansoor Ali, Iyad Dayoub, Sonia Aïssa
Writing – original draft: Rajesh Anbazhagan, S. Chandru
Writing – review & editing: Ravikumar Chinthaginjala, Kalapraveen Bagadi, Mohammad Alibakhshikenari, Bal S. Virdee, Syed Mansoor Ali, Iyad Dayoub, Patrizia Livreri, Sonia Aïssa

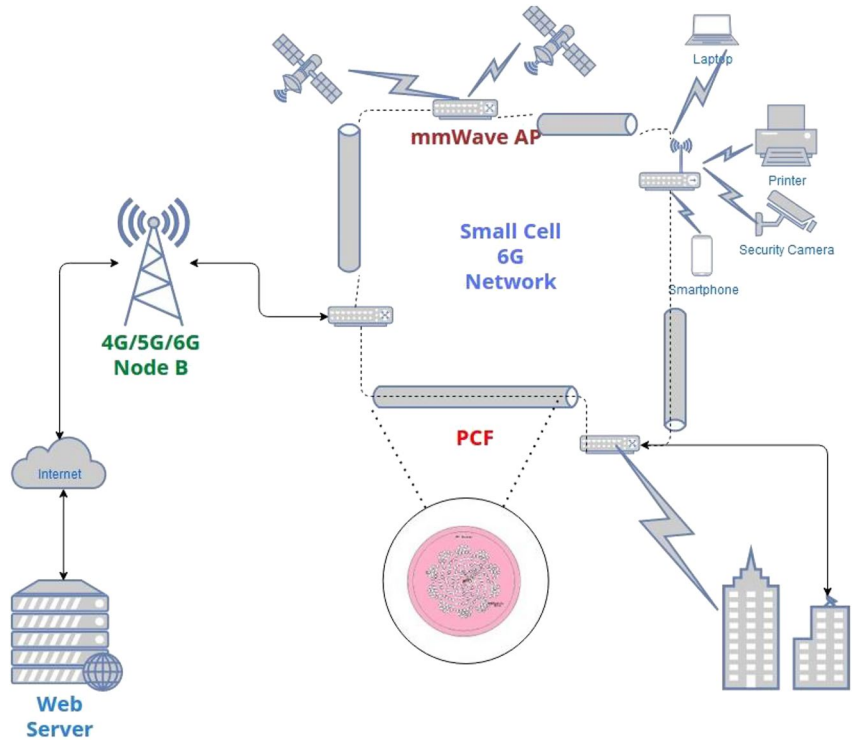

Figure 1. Positioning of proposed spiral flower cladding photonic crystal fiber in 6G networks.

arrangement and finite elements are arranged in triangular lattice. The PCF display a persistent effective area and a high negative dispersion for varying intensity and for the wavelength ranging between 200 and 500 nm.

The authors in (J. Liao, et al., 2017) have designed an ultra-high birefringent PCF by means of elliptical glass rod in core section and spiral arrangement by means of circular air gaps with silica in cladding section. Here, the refractive index of the elliptical rod is kept high as compared to the conventional elliptical structures to exhibit non-linearity of 817.5 W^{-1} km^{-1} with negative dispersion of −491.16 ps/(nm-km). The construction of PCF using arsenic trise-lenide based chalcogenide material has been explored in (J. Li, et al., 2019). The air holes in the cladding region are made up of five layers of concentric rings with uniform air hole and the core region is made up of two layers with

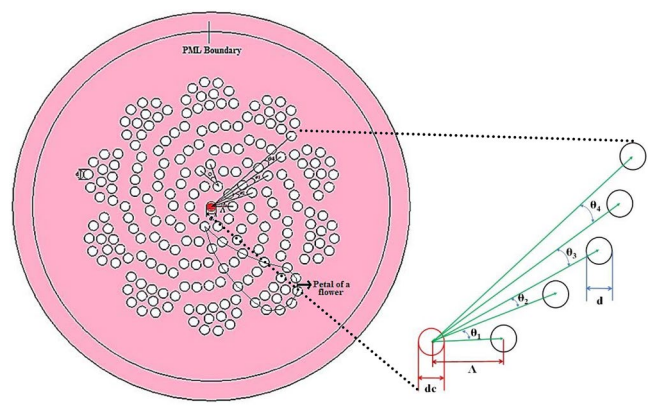

Figure 2. Geometric structure of spiral shaped flower pattern cladding photonic crystal fiber.

1944799x, 2023, 9, Downloaded from https://agupubs.onlinelibrary.wiley.com/doi/10.1029/2023RS007690 by Cochrane France, Wiley Online Library on [13/10/2023]. See the Terms and Conditions (https://onlinelibrary.wiley.com/terms-and-conditions) on Wiley Online Library for rules of use; OA articles are governed by the applicable Creative Commons License

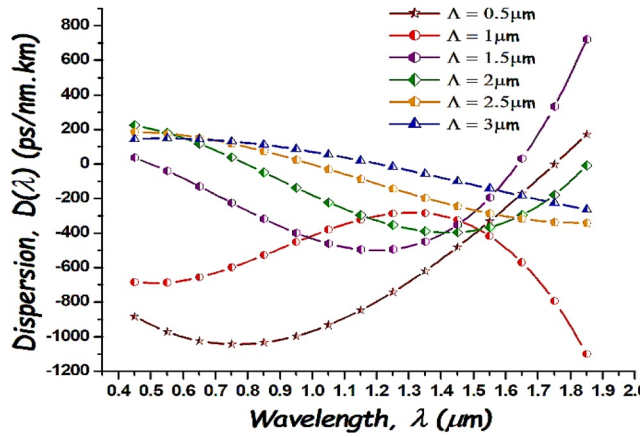

Figure 3. Dispersion performance of flower-cladding photonic crystal fiber for various magnitudes of pitch.

asymmetric air holes and micro concentric rings. The choice of chalcogenide glass is due to its nonlinear refractive index property at the mid-infrared range. The structure generates a broadband supercontinuum at the mid-infrared range (3,887 nm) with a 4 mm PCF that is driven by 100 fs laser pulse with a peak power of 10 kW.

To control the pulse shaping in the process of supercontinuum generation, optimization rule by means of genetic algorithm has been discussed in (M. L. Michaeli & A. Bahabad, 2018). The main advantage with the pulse shaping is the tuning of the spectrum with Gaussian like characteristics. Here, the shaping of pulse prior to feeding the PCF enable the functionality of tunable supercontinuum generation. The tunable source finds its application in realizing broad optical bandwidth and four wave mixing applications with a single laser source (T. Eltaif, 2017). A hybrid PCF with circular and hexagonal planning of air holes in cladding section and elliptical hole with silicon nano rod in core region has been discussed in (Paul, Ahmed, et al., 2018; Paul, Khalek, et al., 2018; Paul, Rajesh, et al., 2018). The PCF exhibits a non-linearity of 1.28×10^{6} W^{-1} km^{-1}in 500 nm. The confinement loss with hybrid PCF is flattened for a wavelength between 500 and 1,800 nm. However, the confinement loss increases exponentially for a wavelength between 1900 and 2,500 nm. The hybrid structure is viable for shorter wavelengths due to reduced scattering loss.

To reduce the confinement loss and scattering loss with high non-linearity, a chalcogenide entrenched quasi PCF have been discussed in (Paul, Ahmed, et al., 2018; Paul, Khalek, et al., 2018; Paul, Rajesh, et al., 2018). The cladding section of PCF is fused with silica and the core region with elliptical holes is fused with chalcogenide. The choice of silica and chalcogenide is the optical transmittance and non-linearity, respectively of the chosen material. The PCF exhibits a non-linearity of 4.72×10^{4} W^{-1} km^{-1} at 1,000 nm for a numerical aperture of 0.85 and scattering loss of 1.92×10^{-8} dB/km. To simplify the fabrication process, a hexagonal structured PCF

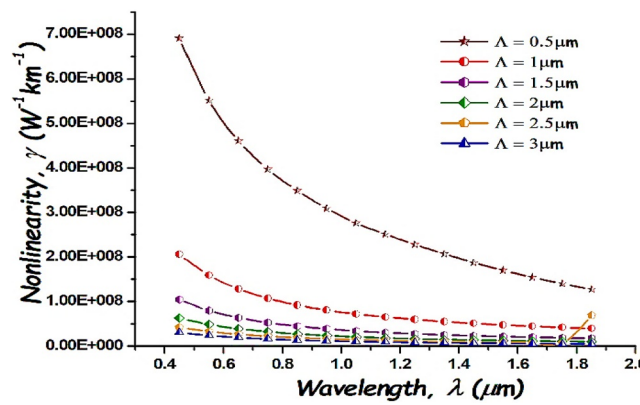

Figure 4. Nonlinearity of the flower-cladding photonic crystal fiber for various magnitudes of pitch.

1944799x, 2023, 9, Downloaded from https://agupubs.onlinelibrary.wiley.com/doi/10.1029/2023RS007690 by Cochrane France, Wiley Online Library on [13/10/2023]. See the Terms and Conditions (https://onlinelibrary.wiley.com/terms-and-conditions) on Wiley Online Library for rules of use; OA articles are governed by the applicable Creative Commons License

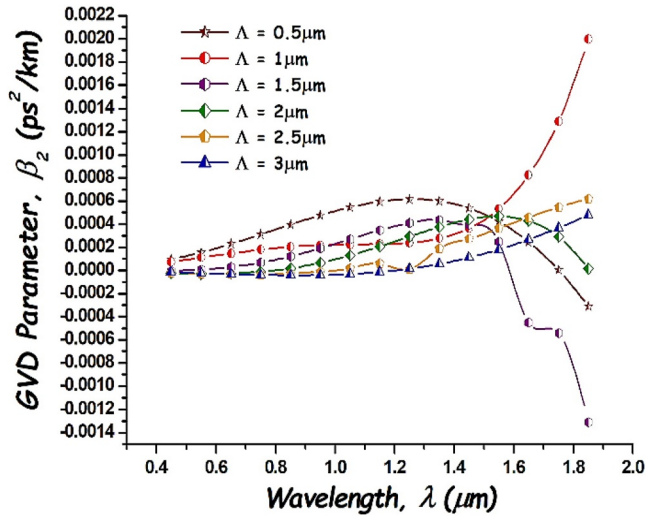

Figure 5. Group-velocity dispersion of flower-cladding photonic crystal fiber for various magnitudes of pitch.

with circular air cavities has been reported (S. K. Biswas, et al., 2018). The PCH structure displays hexagonal symmetry with the introduction of isosceles triangular lattice with fused silica. The PCF exhibits a non-linearity of 96.51 W^{-1} km^{-1} with a negative dispersion of −753.20 ps/nm-km. Alternatively, a complex arrangement of circular and elliptical rings in cladding region with square lattice arrangement has been discussed in (M. I. Islam, et al., 2017). The complex structure provides a non-linearity of 131.91 W^{-1} km^{-1} and negative dispersion of −584.60 ps/nm-km.

Supercontinuum generation in PCF with novel guidance properties has made the spectrum broadening a practically feasible solution. From the results reported in literature (A. Rajesh et al., 2021), it is clear that PCF has made a remarkable development in both technical and essential studies of nonlinear optics. In concert, it also paved the way for developing novel and flexible instruments commercially and it also pursues to instigate the various technical fields. The range of the power of the pump is the most important challenge in solid-core PCF. Thus, the proposed PCF is designed with an optimized dispersion profile to provide the sources with high-power pulses. The profile of the dispersion is tuned by optimizing the design constraints, namely, core structure, diameter of the air-holes, distance among two successive air-holes, air-hole to air-hole gap (Λ) and normalized parameter or

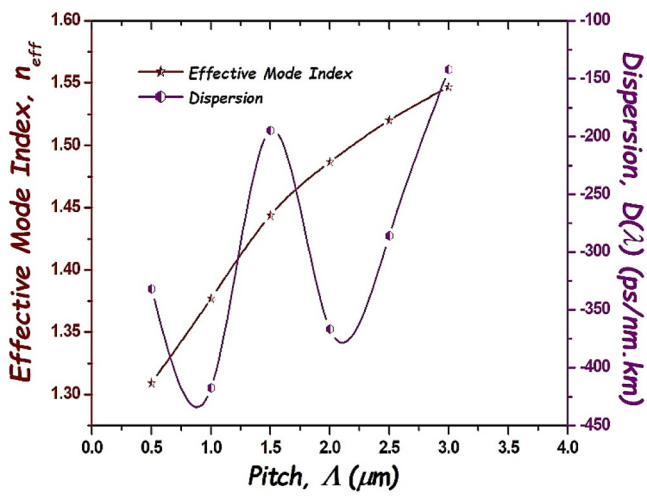

Figure 6. Impact of pitch on effective mode index and dispersion.

1944799x, 2023, 9, Downloaded from https://agupubs.onlinelibrary.wiley.com/doi/10.1029/2023RS007690 by Cochrane France, Wiley Online Library on [13/10/2023]. See the Terms and Conditions (https://onlinelibrary.wiley.com/terms-and-conditions) on Wiley Online Library for rules of use; OA articles are governed by the applicable Creative Commons License

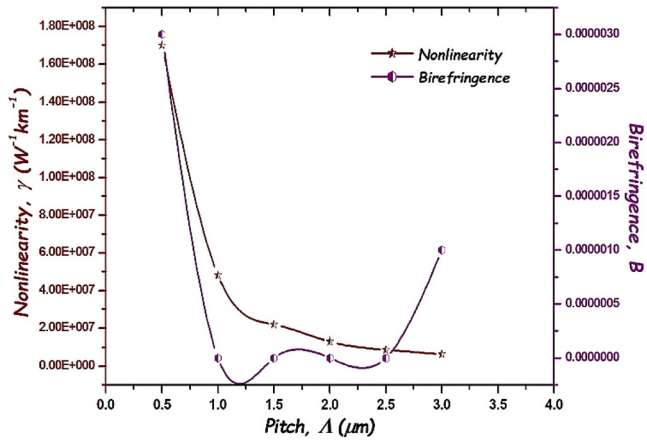

Figure 7. Effect of pitch on nonlinearity and birefringence.

air-filling fraction (d/Λ). Moreover, distribution pattern of structural analysis of air-holes in cladding region has been investigated in detail to optimize the nonlinear properties of the proposed fiber.

It is evident from the above discussion that supercontinuum generation using PCF results in optical spectrum broadening. For effective broadening of the spectrum, the structure of PCF must be optimized to realize low dispersion (≤zero), high nonlinearity (in the order $\geq 10^2$ W^{-1} km-1) with desired birefringence (polarization). The birefringence must be high as the linearly polarized light waves entering the core of an anisotropic fiber splits into two distinct polarized modes propagating with differing velocity orthogonally.

The reminder of the paper is detailed as follows: Section 2 discusses the requirement of the proposed structure in 6G networks with its structural analysis. Section 3 details the performance parameter of the proposed PCF. Section 4 tabulates the numerical comparison of the proposed structure and the works reported in literature. Finally, Section 5 concludes the important discoveries and applications of proposed structure.

2. Proposed Design of Fused Photonic Crystal Fiber

The research was carried out by employing anisotropic PML in finite element method to acquire the effective mode index, n_{eff}. This extends the dynamic features of the PCF comprises of dispersion factor, birefringence, and non-linear aspect (W. Wang, et al., 2020). Modifying the values of the design parameters, namely, the magnitude

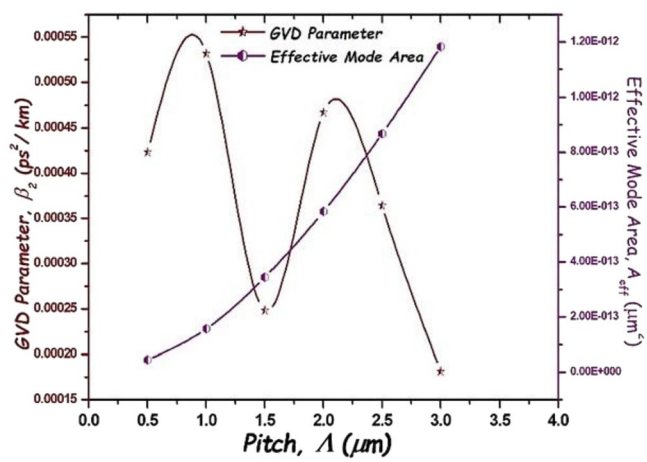

Figure 8. Effect of pitch on group-velocity dispersion and effective mode area.

1944799x, 2023, 9, Downloaded from https://agupubs.onlinelibrary.wiley.com/doi/10.1029/2023RS007690 by Cochrane France, Wiley Online Library on [13/10/2023]. See the Terms and Conditions (https://onlinelibrary.wiley.com/terms-and-conditions) on Wiley Online Library for rules of use; OA articles are governed by the applicable Creative Commons License

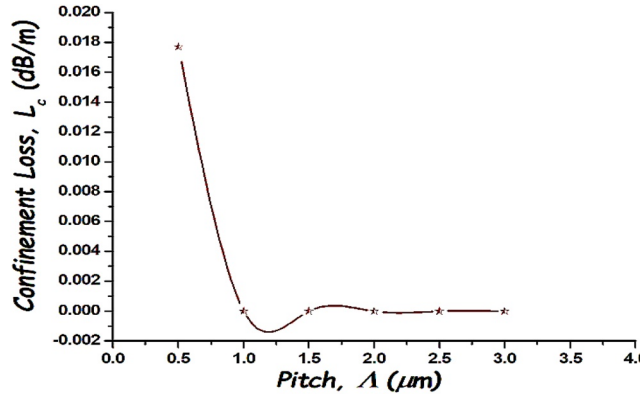

Figure 9. Impact of pitch on confinement loss.

of air-holes and pitch display has an implausible effect on the properties. The refractive index as a function of the wavelength is given by Sellmeier's equation (A. A. Rifat, et al., 2019),

$$n^2(\lambda) = 1 + \frac{S_1}{1 - \left(\frac{T_1}{\lambda^2}\right)} + \frac{S_2}{1 - \left(\frac{T_2}{\lambda^2}\right)} + \frac{S_3}{1 - \left(\frac{T_3}{\lambda^2}\right)} \tag{1}$$

where the Sellmeier's constants, that is, S_1, S_2, S_3 and T_1, T_2, T_3 are quantified methodically, λ denotes the wavelength, n represents the refractive index of contextual material. The effective mode index of PCF can be determined from (Paul, Ahmed, et al., 2018; Paul, Khalek, et al., 2018; Paul, Rajesh, et al., 2018),

$$n_{\text{eff}} = \beta / k_0 \tag{2}$$

where β refers to the propagation constant, and the free space wavenumber is k_0.

The components of the incident pulse propagate through the waveguide at different speeds that expand and distort the rectangular pulse shape referred to as dispersion or pulse broadening (M. M. Faruk, et al., 2019). Pulse propagation and the parameters of the waveguide alters the rate of the dispersion coefficient that varies between zero and a negative value. Dispersion can be restrained by altering the structural parameters, namely, pitch and air-hole

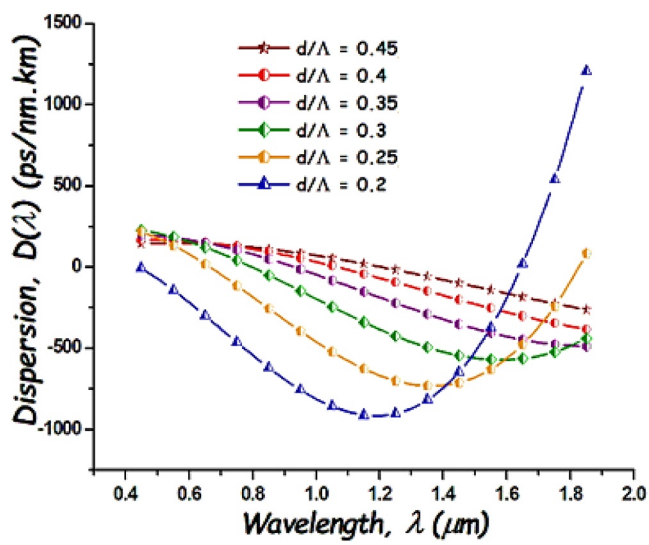

Figure 10. Dispersion properties of flower-cladding photonic crystal fiber for various air-filling fraction.

1944799x, 2023, 9, Downloaded from https://agupubs.onlinelibrary.wiley.com/doi/10.1029/2023RS007690 by Cochrane France, Wiley Online Library on [13/10/2023]. See the Terms and Conditions (https://onlinelibrary.wiley.com/terms-and-conditions) on Wiley Online Library for rules of use; OA articles are governed by the applicable Creative Commons License

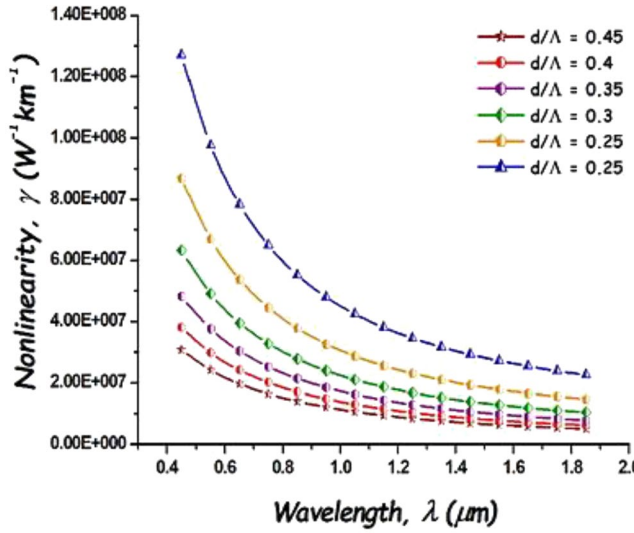

Figure 11. Nonlinearity properties of flower-cladding photonic crystal fiber for various air-filling fraction.

size (M. J. B. M. Leon, et al., 2021). The combination of material dispersion (D_m) with waveguide dispersion (D_w) rovides the amount of dispersion $D(\lambda)$ defined by (T. Yang, et al., 2021),

$$D(\lambda) = D_m + D_w = \frac{-\lambda}{c}\frac{\partial^2 \mathrm{Re}(n_{\mathrm{eff}})}{\partial \lambda^2} \tag{3}$$

where the real part of effective mode index is represented by $\mathrm{Re}(n_{\mathrm{eff}})$.

The throughput and latency requirement of 6G communication systems and networks will enable the convergence of optical and wireless technologies for holistic approach of device connectivity (H. R. D. Filgueiras, et al., 2023). The evolution of higher wireless bands in 6G systems in THz bands will increase the channel capacity of core network. This motivates the inclusion of PCF in fronthaul, middle haul and backhaul of the radio access network. As compared to the conventional microwave circuits, the integrated microwave photonics meet

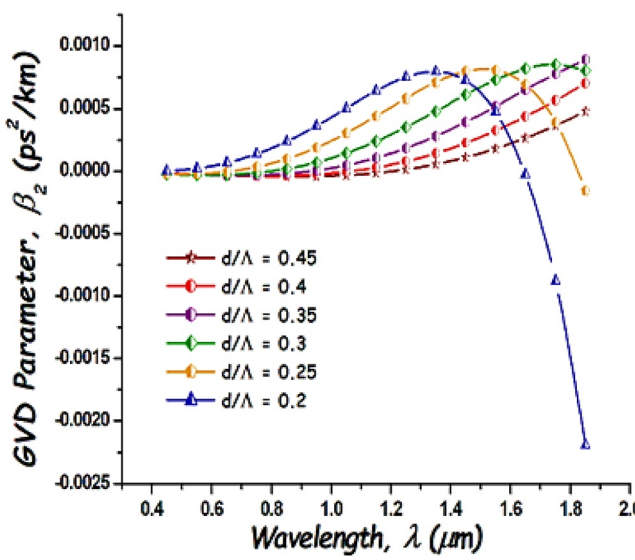

Figure 12. Group-velocity dispersion performance of flower-cladding photonic crystal fiber for various air-filling fraction (d/Λ).

1944799x, 2023, 9, Downloaded from https://agupubs.onlinelibrary.wiley.com/doi/10.1029/2023RS007690 by Cochrane France, Wiley Online Library on [13/10/2023]. See the Terms and Conditions (https://onlinelibrary.wiley.com/terms-and-conditions) on Wiley Online Library for rules of use; OA articles are governed by the applicable Creative Commons License

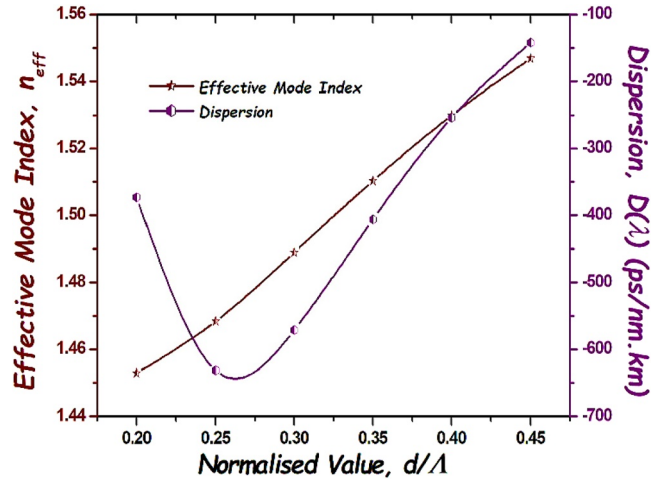

Figure 13. Impression of air-filling section on effective mode index and dispersion.

the requirements of multi-wavelength transmission with PCF supercontinuum generation for 6G networks. This will enable baseband data transmission over the fronthaul 6G fiber network allowing data rates of better than 25 GB/s per channel. For terabit data rate considerations in 6G systems, photonics-based transceivers systems have been developed at middle haul networks (M. Sung, et al., 2021). It includes free running optical source at the transmitter, optical amplifier, supercontinuum PCF at the channel and envelope detection at the receiver. The design of multi-core fiber or PCF for backhaul network using transition technologies has been reported in (T. R. Raddo, et al., 2021) for 6G networks. The major variations in 6G network realization are the deployment of fiber to the antenna section using supercontinuum enabled PCF with high birefringence. Further, the key 6G enablers of optical technologies for mobile transport network include, reconfigurable Mach Zehnder Modulators, and optical dispersion compensator (P. Iovanna, et al., 2021). These devices enable the deployment of optical hub over optical distribution fibers for 100 Gb/s in the downstream. To support such data transmission, a wavelength separation of 2.4 nm with a chromatic dispersion of 170 ps/nm and polarization insensitivity is required (S. R. Moon, et al., 2021).

Various techniques have been reported to optimize generation of supercontinuum in 6G networks that includes the use of air-holes with nonuniform size and hybrid type arrangement of air-holes, as shown in Figure 2. In this paper, supercontinuum has been generated with the pumping power of 20 kW. Further, to generate supercontinuum with high pumping power, innovative structures of PCF have been designed and analyzed. The innovation in

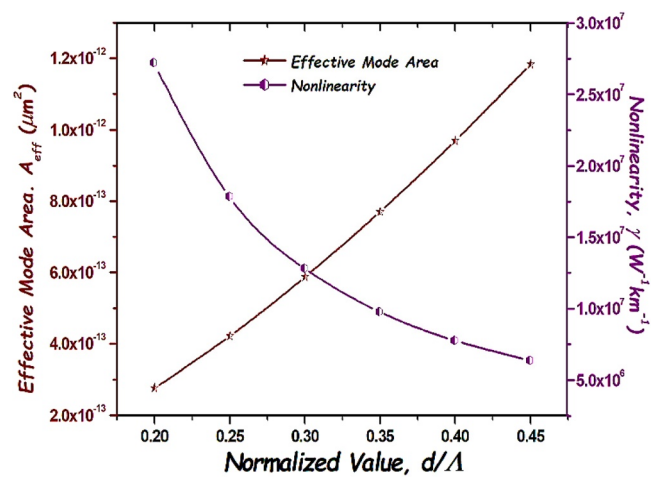

Figure 14. Influence of air-filling segment on effective mode index and nonlinearity.

19447973x, 2023, 9, Downloaded from https://agupubs.onlinelibrary.wiley.com/doi/10.1029/2023RS007690 by Cochrane France, Wiley Online Library on [13/10/2023]. See the Terms and Conditions (https://onlinelibrary.wiley.com/terms-and-conditions) on Wiley Online Library for rules of use; OA articles are governed by the applicable Creative Commons License

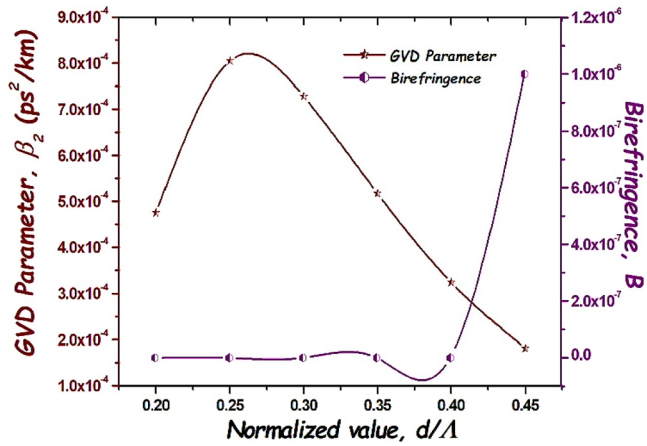

Figure 15. Influence of air-filling segment on group-velocity dispersion parameter and birefringence.

the structure is that the cladding part is constructed with the inspiration from nature in the shape of flower petals. Apart from the optical characteristics that are discussed in conventional designs, the focus on confinement loss is investigated in this paper as the potential application of the proposed structure is to connect the mmWave Access Points, as illustrated in Figure 1. The loss is calculated by introducing the cladding part of the fiber which determines the imaginary part of n_{eff}. Here, the optical parameters are investigated by changing the design constraints, namely, air-filling fraction (d/Λ), pitch (Λ), and core diameter (d_c). The core material is the same as that used in the previous structures of the PCF.

Figure 2 illustrates the flower shaped cladding PCF in which air-holes are arranged in a petal shape. The cladding consists of 10 petals with air-holes of 1.35 μm diameter. Each petal consists of two spiral arms in which the angular displacement of air-holes in first arm can be calculated using $\theta_n = n180°/\text{N}$, where N refers to number of petal rings. Whereas the angular displacement denoted as θ of the air-holes is 30°. The air-holes in the semi-circular part of each petal are displaced with respect to the last row of that petal. The diameter of core is represented by d_c and ranges between 0.6 and 1.35 μm in steps of 0.15 μm. Here, distance between two successive air-holes namely pitch, Λ, is varied from 0.5 to 3 μm in a step of 0.5 μm. For the air-filling section to maintain the single-mode of propagation, its value must be such that $d/\Lambda \leq 0.45$. We have altered the dimension of the air-filled hole to see how this parameter affects the performance of the PCF. We have used the same background and core materials,

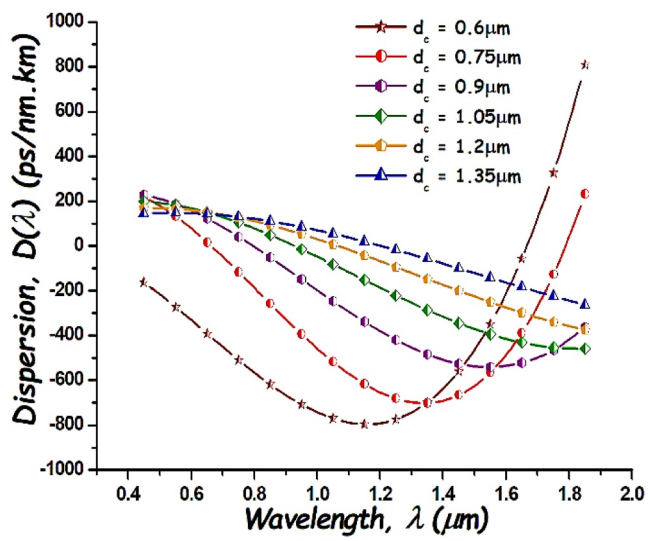

Figure 16. Dispersion of flower-cladding photonic crystal fiber for various core diameters.

1944799x, 2023, 9, Downloaded from https://agupubs.onlinelibrary.wiley.com/doi/10.1029/2023RS007690 by Cochrane France, Wiley Online Library on [13/10/2023]. See the Terms and Conditions (https://onlinelibrary.wiley.com/terms-and-conditions) on Wiley Online Library for rules of use; OA articles are governed by the applicable Creative Commons License

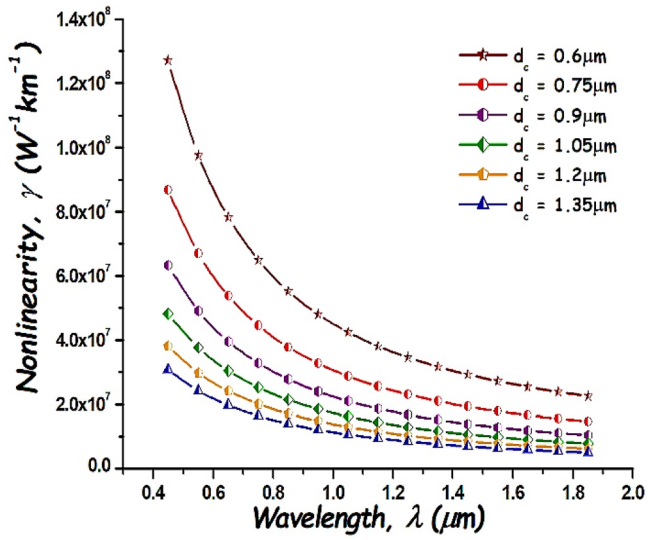

Figure 17. Nonlinearity of flower-cladding photonic crystal fiber for various core diameters.

that is, silica and silicon nanocrystal, respectively, as in the previous works to maintain the stability in the performance characteristics of the fiber,

The coefficient of nonlinearity is the metric used to determine the various nonlinear effects that are responsible for the generation of supercontinuum (T. Baselt, et al., 2017). As discussed earlier, pulse broadening in upcoming 6G applications requires the non-linear coefficient (γ) to be as high as possible. Such requirement is obtained by using a source of high intensity at the core region of reduced effective mode area (A_{eff}). The non-linear coefficient is given by (M. S. Rao & V. Singh, 2018),

$$\gamma = \frac{2\pi n_2}{\lambda A_{\text{eff}}} \tag{4}$$

where n_2 specifies non-linear refractive index. Effective mode area can be calculated using (M. Seifouri, & M. R. Alizadeh, 2018),

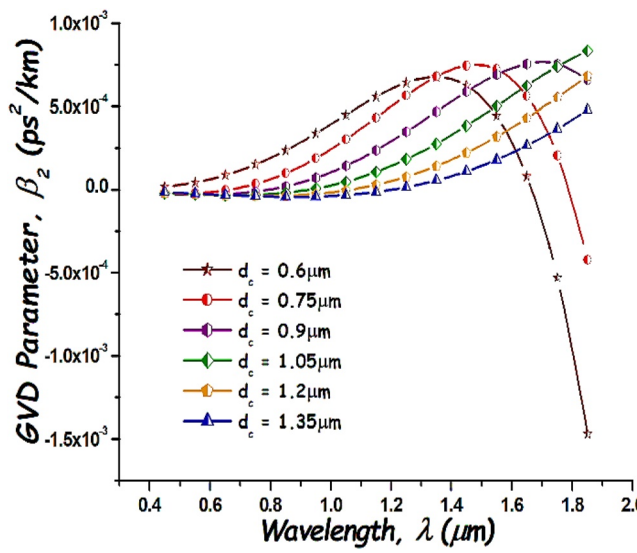

Figure 18. Group-velocity dispersion of flower-cladding photonic crystal fiber for various core diameters.

1944799x, 2023, 9, Downloaded from https://agupubs.onlinelibrary.wiley.com/doi/10.1029/2023RS007690 by Cochrane France, Wiley Online Library on [13/10/2023]. See the Terms and Conditions (https://onlinelibrary.wiley.com/terms-and-conditions) on Wiley Online Library for rules of use; OA articles are governed by the applicable Creative Commons License

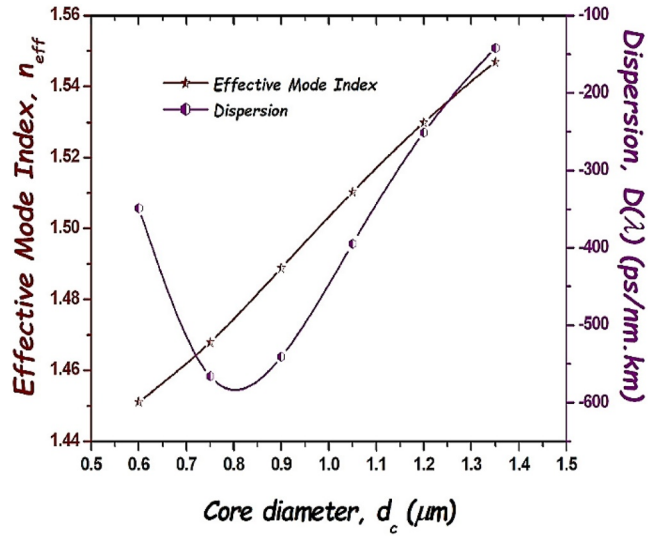

Figure 19. Impact of core diameter on effective mode index with dispersion.

$$A_{\text{eff}} = \frac{\left[\int_{-\infty}^{\infty}\int_{-\infty}^{\infty} |E(x,y)|^2 dx\, dy\right]^2}{\int_{-\infty}^{\infty}\int_{-\infty}^{\infty} |E(x,y)|^4 dx\, dy} \tag{5}$$

where $E(x,y)$ refers to electric field mode distribution of fundamental fiber mode. Birefringence introduces a difference in refractive index (M. A. Gandhi, et al., 2017; M. Kalantari, et al., 2018). The difference in the real part of n_{eff} of two polarized modes, which is referred to as modal birefringence, can be determined from (H. Saghaei, 2017; G. M. Zheng, 2021),

$$B = \left|\text{Re}\left(n_{\text{eff}}^{x}\right) - \text{Re}\left(n_{\text{eff}}^{y}\right)\right| \tag{6}$$

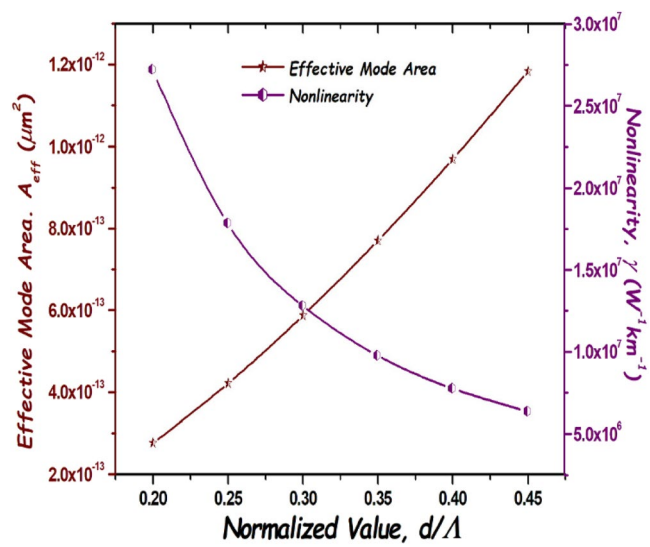

Figure 20. Impact of core diameter on effective mode index with nonlinearity.

1944799x, 2023, 9, Downloaded from https://agupubs.onlinelibrary.wiley.com/doi/10.1029/2023RS007690 by Cochrane France, Wiley Online Library on [13/10/2023]. See the Terms and Conditions (https://onlinelibrary.wiley.com/terms-and-conditions) on Wiley Online Library for rules of use; OA articles are governed by the applicable Creative Commons License

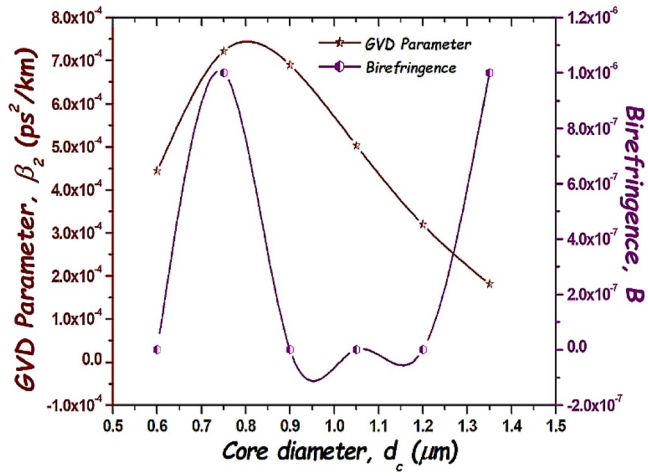

Figure 21. Impact of core diameter on group-velocity dispersion parameter and birefringence.

where $\mathrm{Re}\left(n_{\mathrm{eff}}^{x}\right)$ and $\mathrm{Re}\left(n_{\mathrm{eff}}^{y}\right)$ are the real parts of n_{eff} in the x and y directions, respectively. Ideally, the light waves would be totally confined in the core of proposed PCF if the cladding has infinite periodic rings of microstructures. However, in reality the PCF cladding will consist of a limited number of rings of microstructures. As a result, a fraction of the optical pulse power will escape from the structure. Such leakage is characterized by confinement loss, which can be deduced from (A. M. I. Aaidi, et al., 2021; A. Habib, et al., 2021),

$$L_c = 8.686k\, Im(n_{\mathrm{eff}}) \tag{7}$$

where $k = 2\pi/\lambda$ is a free space wave number, and $Im(n_{\mathrm{eff}})$ refer to imaginary part of n_{eff}. The surface of an optical pulse propagates at the group velocity (v_g) that depends on the frequency or wavelength whereas the parameter β_2 indicates the dispersion of the group velocity and it is highly involved in the broadening of an optical pulse (T. L. Courtney, et al., 2021; Dhara & Singh, 2021). This process is generally known as group-velocity dispersion (GVD) and β_2 is termed as GVD parameter. Its value may be either positive or negative and it depends on the position of wavelength with respect to the zero-dispersion wavelength. Group-velocity dispersion can be calculated using (R. Salgueiro, & A. Ferrando, 2018; D. Xiong, et al., 2021),

$$\mathrm{GVD} = \frac{-2\pi c}{\omega^2} \times D(\lambda) \tag{8}$$

where c is the speed of light, ω is the angular frequency, and D signifies the dispersion coefficient.

3. Results and Discussion

The variation of dispersion in proposed PCF for various values of pitch and a function of wavelength is shown in Figure 3. It is evident from the figure that the dispersive property of the PCF for lower pitch values ranging from 0.5 to 2 μm oscillates between a positive and a negative value. In this range of pitch, the fiber exhibit a negative dispersion value of −417.2 ps/(nm.km) at pitch value of 1 μm. Further, a reduced negative dispersion value corresponding to −194.7 ps/(nm.km) the pitch value obatined is 1.5 μm at a wavelength of about 1.55 μm. But for higher pitch values of about 2.5 and 3 μm, the dispersive property of the fiber reduces from positive to a negative value. In this range of pitch, at a wavelength of about 1.55 μm the fiber provides a degraded dispersion value of −285.8 ps/(nm.km) at pitch value of 2.5 μm, and dispersion of −142.1 ps/(nm.km) at pitch value of 3 μm. Here, the zero-dispersion wavelength of the proposed PCF is about 1.2 μm.

Nonlinear properties of the proposed PCF reduces with increasing pitch, as shown in Figure 4. At $\lambda = 1.55$ μm, it offers a very high nonlinearity of about 1.70×10^8 W^{-1} km^{-1} for a low pitch value of 0.5 μm. For the higher pitch value ranging from 1 to 2 μm, the nonlinearity is almost constant and is in the order of 10^7 W^{-1} km^{-1}. The nonlinearity is 4.8×10^7 W^{-1} km^{-1} for a pitch 1 μm at $\lambda = 1.55$ μm. Whereas, for the pitch values of about 2.5 and 3 μm, the proposed structure provides nonlinearity in the order of 10^6 W^{-1} Km^{-1}. For a pitch of 2.5 μm, the nonlinearity is

1944799x, 2023, 9, Downloaded from https://agupubs.onlinelibrary.wiley.com/doi/10.1029/2023RS007690 by Cochrane France, Wiley Online Library on [13/10/2023]. See the Terms and Conditions (https://onlinelibrary.wiley.com/terms-and-conditions) on Wiley Online Library for rules of use; OA articles are governed by the applicable Creative Commons License

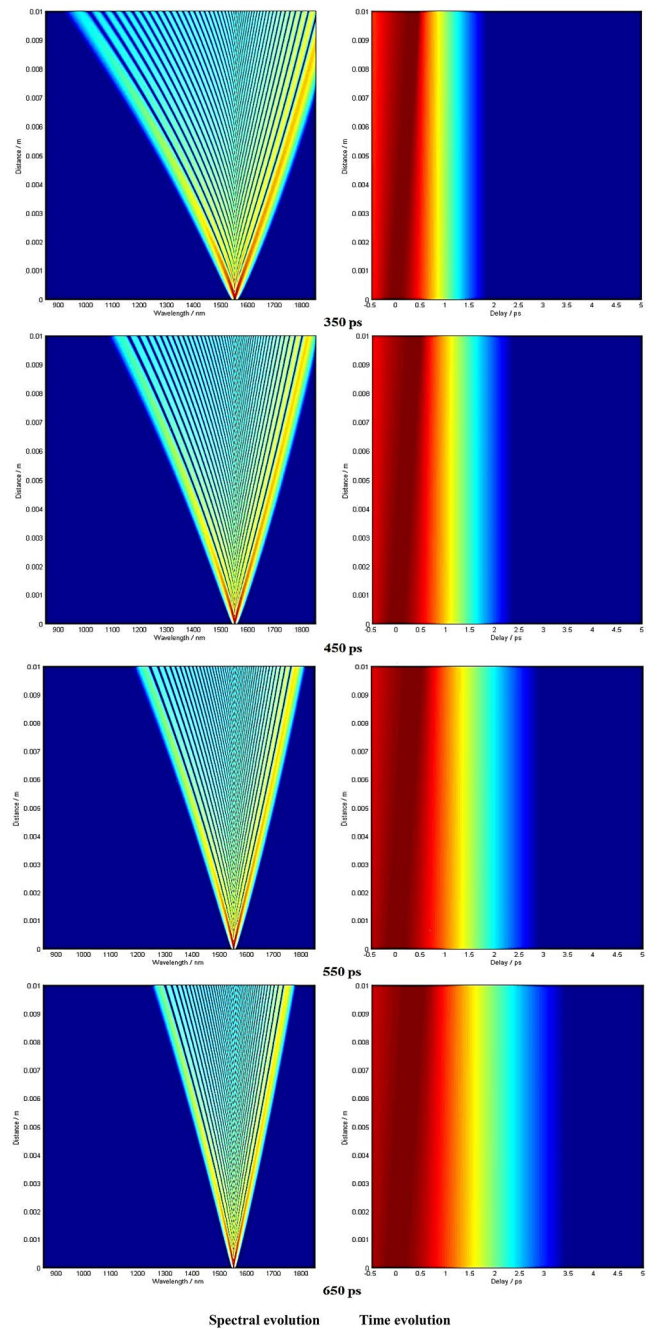

Figure 22. Spectral and time evolution of supercontinuum generation for 10 mm photonic crystal fiber.

about 8.69×10^6 W^{-1} km^{-1}, and for a pitch of 3 μm it is about 1.7×10^6 W^{-1} km^{-1} at $\lambda = 1.55$ μm. Figure 5 shows how the GVD parameter (β_2) value changes from a positive to a negative value for the low pitch values ranging from 0.5 to 2 μm. The GVD has a very low value of about -6.11×10^{-5} ps^2/km for a pitch of 0.5 μm, and a comparatively high value of about 2.48×10^{-4} ps^2/km at $\lambda = 1.55$ μm. But for the high pitch values of about 2.5 and 3 μm, the GVD value increases from a low value to high value. For a pitch 1 μm, the GVD of the fiber is about 3.64×10^{-4} ps^2/km and a comparatively low value of about 1.811×10^{-4} ps^2/km for a pitch of 3 μm at a wavelength of 1.55 μm.

The characteristics of proposed PCF for various pitch values is shown in Figures 6–9. It is evident that the fiber provides a very high birefringence of about 3×10^{-6} for a pitch value of 0.5 μm. The birefringence is 1×10^{-6} at $\lambda = 1.55$ μm for a pitch of 3 μm. For a pitch of 3 μm, the fiber behaves as a lossless fiber, that is, the confine-

1944799x, 2023, 9, Downloaded from https://agupubs.onlinelibrary.wiley.com/doi/10.1029/2023RS007690 by Cochrane France, Wiley Online Library on [13/10/2023]. See the Terms and Conditions (https://onlinelibrary.wiley.com/terms-and-conditions) on Wiley Online Library for rules of use; OA articles are governed by the applicable Creative Commons License

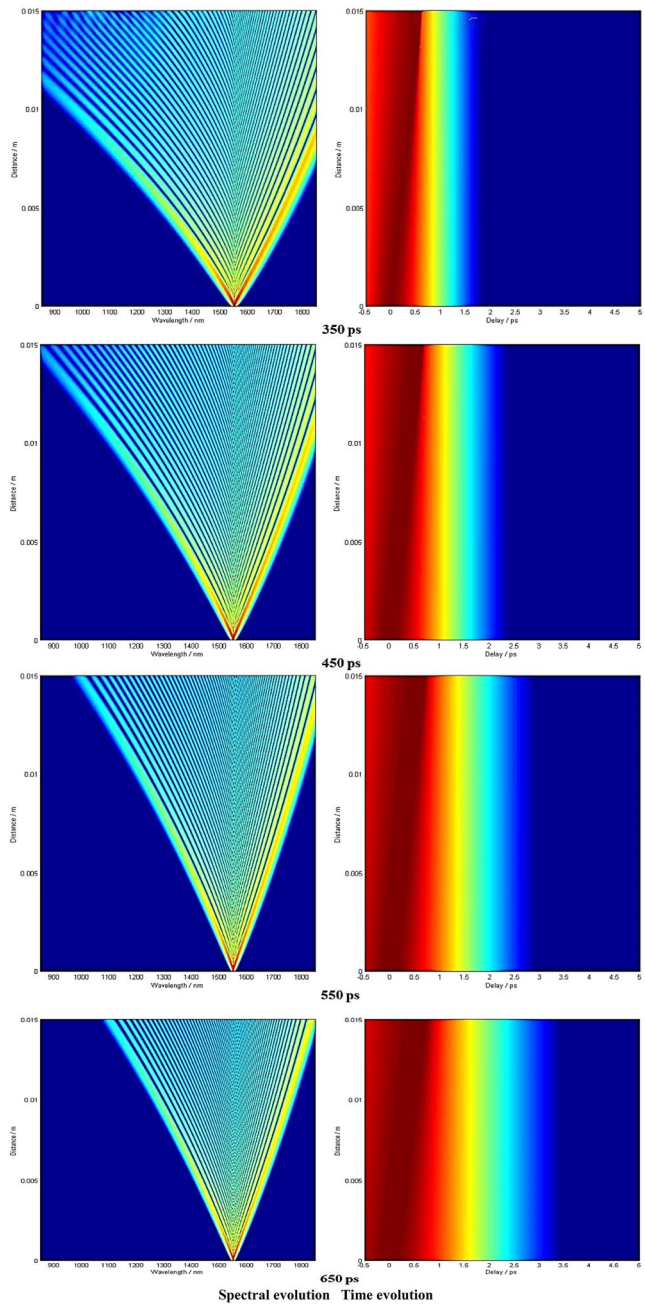

Figure 23. Spectral and time evolution of supercontinuum generation for 15 mm photonic crystal fiber.

Table 1
Performance Parameters of Flower-Cladding Photonic Crystal Fiber for Various Pitch

Λ (μm)	n_{eff}	$D(\lambda)$ (ps/nm.km)	A_{eff} (μm^2)	γ (W^{-1} km^{-1})	B	Lc (dB/m)	β_2 (ps^2/km)
0.5	1.309213	−331.9	0.0443E^{-12}	1.70E^{8}	6.95E^{-6}	1.77E^{-2}	−6.109E^{-5}
1	1.377086	−417.2	0.1572E^{-12}	4.796E^{7}	0	2.03E^{-7}	5.318E^{-4}
1.5	1.443845	−194.7	0.3447E^{-12}	2.19E^{7}	0	0	2.482E^{-4}
2	1.486772	−366.6	0.5843E^{-12}	1.19E^{7}	0	0	4.672E^{-4}
2.5	1.520189	−285.8	0.8675 E^{-12}	8.69E^{6}	0	0	3.642E^{-4}
3	1.546877	−142.1	1.1833 E^{-12}	1.70E^{6}	0	0	1.811E^{-4}

1944799x, 2023, 9, Downloaded from https://agupubs.onlinelibrary.wiley.com/doi/10.1029/2023RS007690 by Cochrane France, Wiley Online Library on [13/10/2023]. See the Terms and Conditions (https://onlinelibrary.wiley.com/terms-and-conditions) on Wiley Online Library for rules of use; OA articles are governed by the applicable Creative Commons License

1944799x, 2023, 9, Downloaded from https://agupubs.onlinelibrary.wiley.com/doi/10.1029/2023RS007690 by Cochrane France, Wiley Online Library on [13/10/2023]. See the Terms and Conditions (https://onlinelibrary.wiley.com/terms-and-conditions) on Wiley Online Library for rules of use; OA articles are governed by the applicable Creative Commons License

Table 2
Performance Parameters of Flower-Cladding Photonic Crystal Fiber for Various Air-Filling Fraction

d/Λ	n_{eff}	$D(\lambda)$ (ps/nm.km)	A_{eff} (μm^2)	γ (W^{-1} km^{-1})	B	Lc (dB/m)	β_2 (ps^2/km)
0.2	1.45295	−372.8	$0.2769E^{-12}$	$2.723E^{7}$	0	0	$4.752E^{-4}$
0.25	1.46837	−631.3	$0.4218E^{-12}$	$1.788E^{7}$	0	0	$8.047E^{-4}$
0.3	1.488933	−571.2	$0.5874E^{-12}$	$1.284E^{7}$	0	0	$7.28E^{-4}$
0.35	1.510283	−406	$0.7703E^{-12}$	$9.788E^{7}$	0	0	$5.174E^{-4}$
0.4	1.529877	−254.2	$0.9691E^{-12}$	$7.780E^{6}$	0	0	$3.24E^{-4}$
0.45	1.546877	−142.1	$1.1833E^{-12}$	$6.37E^{6}$	$1E^{-6}$	0	$1.811E^{-4}$

ment loss of the propagation is zero. From this analysis, it is concluded that for an efficient generation of SC, the pitch value of about 3 μm is suitable because it provides a fiber with low and negative dispersion, high non-linearity, low birefringence, and a zero confinement loss. It is found that the behavior of optical constraints in flower-cladding PCF varies with air-filling fraction (d/Λ). The variation of dispersion with reference to different values of d/Λ is shown in Figure 10. Here, the dispersive property of the fiber changes between the low and high value with an increase in d/Λ from 0.2 to 0.45. For lower wavelengths, the dispersion is near to zero and for longer wavelengths, it exhibits a high positive dispersion. At $\lambda = 1.55$ μm, the proposed structure exhibits a negative dispersion of −631.3 ps/(nm-km) for $d/\Lambda = 0.25$ and negative dispersion equivalent to −142.1 ps/(nm-km) for $d/\Lambda = 0.45$.

Nonlinear characteristics of the proposed PCF reduces with an increase in d/Λ, as shown in Figure 11. At $\lambda = 1.55$ μm, the d/Λ ranging from 0.2 to 0.35 the nonlinearity is in the order of 10^7 W^{-1} km^{-1}. More specifically, the nonlinearity is about 9.79×10^7 W^{-1} km^{-1} for $d/\Lambda = 0.35$ at a wavelength of 1.55 μm. Whereas, for the values of d/Λ in the range of 0.4 & 0.45, the proposed structure provides nonlinearity in the order of 10^6 W^{-1} km^{-1}. For $d/\Lambda = 0.4$, the proposed PCF has a nonlinearity value of about 7.78×10^6 W^{-1} km^{-1}, and for $d/\Lambda = 0.45$, the nonlinaerity is about 6.37×10^6 W^{-1} km^{-1} at $\lambda = 1.55$ μm. Figure 12 shows the GVD parameter (β_2) value changes between a low and the high value with an increase in d/Λ from 0.2 to 0.45. Here, the β_2 values are positive as the dispersion for all d/Λ values is negative. It provides a low GVD value of about 1.81×10^{-4} ps^2/km for $d/\Lambda = 0.45$, and a comparatively high GVD value of about 8.05×10^{-4} ps^2/km at $\lambda = 1.55$ μm for $d/\Lambda = 0.25$.

The performance characteristics of d/Λ is shown in Figures 13–15. The behavior of dispersion, nonlinearity, and GVD parameter were discussed earlier. It is evident that the fiber provides a very high Birefringence of about 1×10^{-6} at $\lambda = 1.55$ μm for $d/\Lambda = 0.45$. The change in the value of d/Λ doesn't create any loss in the propagation of an incident pulse. That is, the proposed PCF is a lossless fiber. From this analysis, it can be concluded that for an efficient generation of supercontinuum, the d/Λ value of about 0.45 is highly suitable because it provides a fiber with low negative value dispersion and high nonlinearity.

Examined now is the optical constraints of the proposed PCF as a function of core diameter (d_c). Variation of dispersion in the proposed PCF for various d_c is shown in Figure 16. The variation is analogous to the performance features of fiber corresponding to d/Λ. But, the values of the optical parameters obtained above $\lambda = 1.55$ μm

Table 3
Performance Parameters of the Flower-Cladding Photonic Crystal Fiber for Various Core Diameter

d_c (μm)	n_{eff}	$D(\lambda)$ (ps/nm.km)	A_{eff} (μm^2)	γ (W^{-1} km^{-1})	B	Lc (dB/m)	β_2 (ps^2/km)
0.6	1.45295	−348.8	$0.2769E^{-12}$	$2.71E^{7}$	$1E^{-6}$	0	$4.445E^{-4}$
0.75	1.46837	−566.2	$0.4218E^{-12}$	$1.79E^{7}$	0	0	$7.217E^{-4}$
0.9	1.488933	−541.1	$0.5874E^{-12}$	$1.28E^{7}$	0	0	$6.897E^{-4}$
1.05	1.510283	−394.8	$0.7703E^{-12}$	$9.79E^{7}$	0	0	$5.031E^{-4}$
1.2	1.529877	−250.8	$0.9691E^{-12}$	$7.74E^{6}$	0	0	$3.197E^{-4}$
1.35	1.546877	−142.1	$1.1833E^{-12}$	$6.37E^{6}$	$1E^{-6}$	0	$1.811E^{-4}$

Table 4
Comparison of Flower-Cladding Structure With Works in Literature

Parameters	A. Medjouri, et al. (2019)	A. Aparna Nair, et al. (2019)	P. Chauhan, et al. (2018)	P. Chauhan, et al. (2019)	M. Sharma and Konar (2016)	T. Singh Saini et al. (2015)	Proposed work
λ (μm)	4.5	0.850	1.35	4	1.55	4.1	1.55
$D(\lambda)$ (ps/nm.km)	Zero	Zero	−92.08	−19.52 to −11.78	40	-	−142.1
γ (W^{-1} km^{-1})	970	220	884	853	923	1,944	$6.37E^6$
Pulse width T_0 (ps)	0.48	0.49	NA	0.89	0.499	0.499	0.350–0.650
Initial peak power P_0 (kW)	20	1.8	0.00050	8.19	0.00100	3.5	25

exhibit negative dispersion. The dispersion is −566.2 ps/(nm.km) for $d_c = 0.75$ μm and it decreases to −142.1 ps/(nm.km) at $d_c = 1.35$ μm.

In the case of nonlinearity, as shown in Figure 17, it begins to reduce above $\lambda = 1.55$ μm and is in the order of 10^7 W^{-1} km^{-1} for lower d_c values between 0.6 and 1.35 μm. The nonlinearity is about 9.79×10^7 W^{-1} km^{-1} for $d_c = 1.05$ μm at a wavelength of 1.55 μm. Whereas, for the d_c values of 1.2 μm & 1.35 μm, the proposed structure provides nonlinearity in the order of 10^6 W^{-1} km^{-1}. For $d_c = 1.2$ μm, the nonlinearity is about 7.74×10^6 W^{-1} km^{-1} and for $d_c = 1.35$ μm, it is about 6.37×10^6 W^{-1} km^{-1} at $\lambda = 1.55$ μm. The GVD parameter (β_2) is shown in Figure 18. GVD parameter values are positive up $\lambda = 1.7$ μm since the dispersion for all values of d_c is negative. The GVD parameter value is about 1.81×10^{-4} ps^2/km for $d_c = 1.35$ μm and increases to 7.22×10^{-4} ps^2/km at $\lambda = 1.55$ μm for $d_c = 1.35$ μm. The performance of PCF as a function of d_c is shown in Figures 19–21. It is evident that the fiber provides a very high Birefringence of about 1×10^{-6} at $\lambda = 1.55$ μm for two core diameters $d_c = 0.75$ μm & 1.35 μm. The change in the value of core diameter doesn't create any loss in the propagation of an incident pulse. That is, the proposed PCF is a lossless fiber. From Figure 20, can be concluded that for an efficient generation of SC, the d_c value of about 1.35 μm is suitable because it provides a fiber with low negative value dispersion, high nonlinearity, high birefringence, and a zero confinement loss. Finally, can be concluded that for the generation of SC using PCF with $\Lambda = 3$ μm, $d/\Lambda = 0.45$ & $d_c = 1.35$ μm is preferable.

Spectral and temporal evolution of supercontinuum functionality for 10 mm fiber with preliminary maximum power of 25 kW for tetrad pulse dimensions are shown in Figure 22. The spectral and temporal evolution of supercontinuum for the extended 15 mm fiber for various pulse durations are shown in Figure 23. The dispersion distance is calculated using the expression $L_D = T_0^2/|\beta_2|$. The dispersion distance is calculated to vary between 0.68 and 2.33 μm for pulse durations between 350 and 600 ps. Moreover, the nonlinear length can be found using the expression $L_{NL} = 1/\gamma P_0$ and calculated to be 0.0063 μm. Further, soliton numeral N is calculated using $N^2 = L_D/L_{NL}$ and it lies between 10 and 19 for tetrad pulse dimensions.

By transmitting an intense pulse in an abnormal dispersion region, the spectrum is broadened. This spectrum broadening essentially balances the temporal compression due to anomalous dispersion. Here, spectrum broadening is achieved by means of self-phase modulation. The sidebands generated depend on pumping power. The flower-cladding PCF results in spectrum broadening for rapid pulses of duration between 350 and 450 ps, however the expansion is relatively small for stretched pulses corresponding to 550 and 650 ps duration.

4. Numerical Results

The measured optical parameters of the proposed structure are tabulated in Tables 1–3. The dispersive property of the proposed PCF oscillates between a positive and a negative value. Nevertheless, change in core diameter and the change in the air-filling fraction has an almost similar effect on the all-optical parameters. In all variations, the novel PCF exhibits a negative dispersion and its nonlinear properties are achieved in the order of 10^{-7} W^{-1} km^{-1} and 10^{-6} W^{-1} km^{-1}. Here, the novel PCF is highly birefringent, and it is maintained as a lossless fiber throughout its propagation at $\lambda = 1.55$ μm.

Finally, based on the observations, it is concluded that PCF with $\Lambda = 3$ μm, $d/\Lambda = 0.45$ & $d_c = 1.35$ μm is highly suitable for the generation of supercontinuum. This is because the proposed PCF, which is designed with these parameters, exhibits a reduced negative dispersion, a increased nonlinearity, high birefringence, and a zero confinement loss. The optical constraints of the proposed flower-cladding PCF are compared with several other PCF structures in Table 4. Compared to other structures the nonlinearity of the proposed bio-inspired innovative PCF structure is extremely high. But in contrast it has the highest dispersion, which is negative. The supercontinuum generated at 25 kW is relatively higher than that reported in literature. The proposed PCF is designed for application in 6G telecommunication band of 1.55 μm.

5. Conclusion

The design of an innovative structure of PCF has been discussed for supercontinuum generation with high pumping power. Analysis is presented on how the parameters of the photonic crystal structure such as pitch, air-filling fraction, and core diameter influences the performance metrics of the PCF. It is shown that the PCF exhibits a very high birefringence and the confinement loss obtained is zero. The optical pulse has been broadened with

1944799x, 2023, 9, Downloaded from https://agupubs.onlinelibrary.wiley.com/doi/10.1029/2023RS007690 by Cochrane France, Wiley Online Library on [13/10/2023]. See the Terms and Conditions (https://onlinelibrary.wiley.com/terms-and-conditions) on Wiley Online Library for rules of use; OA articles are governed by the applicable Creative Commons License

high pumping power of 25 kW that is applicable for next generation 6G networks. The structural analysis of nano-core PCF with fused cladding will provide a baseline for designing the 6G architecture.

Conflict of Interest

The authors declare no conflicts of interest relevant to this study.

Data Availability Statement

Data were not used, nor created for this research. All of the figures, materials, and data within the manuscript are original and owned by authors.

Acknowledgments
Dr. Mohammad Alibakhshikenari acknowledges support from the CONEX-Plus programme funded by Universidad Carlos III de Madrid and the European Union's Horizon 2020 research and innovation programme under the Marie Sklodowska-Curie grant agreement No. 801538. The authors also sincerely appreciate funding from Researchers Supporting Project number (RSPD2023R699), King Saud University, Riyadh, Saudi Arabia. Besides above, the Article Processing Charge (APC) was afforded by Universidad Carlos III de Madrid (Agreement CRUE-Madrono 2023).

References

Abdullah-Al-Shafi, M., & Sen, S. (2021). Design of a low material loss and larger effective area based photonic crystal fiber for communication applications in terahertz (THz) waveguide. *Sensing and Bio-Sensing Research*, *31*, 100400. https://doi.org/10.1016/j.sbsr.2021.100400

Aparna Nair, A., Boopathi, C. S., Jayaraju, M., & Mani Rajan, M. S. (2019). Numerical investigation and analysis of flattened dispersion for supercontinuum generation at very low power using Hexagonal shaped Photonic crystal fiber (H-PCF). *Optik: International Journal for Light and Electron Optics*, *179*, 718–725. https://doi.org/10.1016/j.ijleo.2018.11.021

Baselt, T., Taudt, C., Nelsen, B., Lasagni, A. F., & Hartmann, P. (2017). February. All-fiber supercontinuum source with flat, high power spectral density in the range between 1.1 μm to 1.4 μm based on an Yb3+ doped nonlinear photonic crystal fiber. In *Nonlinear frequency generation and conversion: Materials and devices XVI* (Vol. 10088, p. 100880E). International Society for Optics and Photonics.

Biswas, S. K., Islam, S. M., Islam, M., Mia, M. M. A., Sayem, S., & Ahmed, F. (2018). September. Design of an ultrahigh birefringence photonic crystal fiber with large nonlinearity using all circular air holes for a fiber-optic transmission system. In *Photonics* (Vol. 5, p. 26). Multidisciplinary Digital Publishing Institute.

Chauhan, P., Kumar, A., & Kalra, Y. (2018). Mid-infrared broadband supercontinuum generation in a highly nonlinear rectangular core chalcogenide photonic crystal fiber. *Optical Fiber Technology*, *46*, 174–178. https://doi.org/10.1016/j.yofte.2018.10.004

Chauhan, P., Kumar, A., & Kalra, Y. (2019). Computational modeling of tellurite based photonic crystal fiber for infrared supercontinuum generation. *Optik: International Journal for Light and Electron Optics*, *187*, 92–97. https://doi.org/10.1016/j.ijleo.2019.03.106

Courtney, T. L., Lopez-Zelaya, C., Amezcua-Correa, R., & Keyser, C. K. (2021). Modeling quasi-phase-matched electric-field-induced optical parametric amplification in hollow-core photonic crystal fibers. *Optics Express*, *29*(8), 11962–11975. https://doi.org/10.1364/oe.420075

Dhara, P., & Singh, V. K. (2021). Investigation of rectangular solid-core photonic crystal fiber as temperature sensor. *Microsystem Technologies*, *27*(1), 127–132. https://doi.org/10.1007/s00542-020-04927-1

Dixit, A., Tiwari, S., & Pandey, P. C. (2017). Optical properties of 3rd order Kerr hexagonal nonlinear photonic crystal fiber containing metal. *International Journal of Modern Physics B*, *31*(8), 1750047. https://doi.org/10.1142/s0217979217500473

Eltaif, T. (2017). Broad optical bandwidth based on nonlinear effect of intensity and phase modulators through intense four-wave mixing in photonic crystal fiber. *Optical Engineering*, *56*(5), 056111. https://doi.org/10.1117/1.oe.56.5.056111

Faruk, M. M., Khan, N. T., & Biswas, S. K. (2019). Highly nonlinear bored core hexagonal photonic crystal fiber (BC-HPCF) with ultra-high negative dispersion for fiber optic transmission system. *Frontiers of Optoelectronics*, *13*(4), 1–8. https://doi.org/10.1007/s12200-019-0948-8

Filgueiras, H. R. D., Lima, E. S., Cunha, M. S. B., Lopes, C. H. D. S., De Souza, L. C., Borges, R. M., et al. (2023). Wireless and optical convergent access technologies toward 6G. *IEEE Access*, *11*, 9232–9259. https://doi.org/10.1109/access.2023.3239807

Gandhi, M. A., Melwin, G., Babu, P. R., Abobaker, A. M., Nakkeeran, K., & Senthilnathan, K. (2017). Generation of few-cycle laser pulses using a photonic quasi-crystal fiber. In *Recent trends in materials science and applications* (pp. 153–158). Springer.

Guo, Y., Yuan, J., Wang, K., Wang, H., Cheng, Y., Zhou, X., et al. (2021). Generation of supercontinuum and frequency comb in a nitrobenzene-core photonic crystal fiber with all-normal dispersion profile. *Optics Communications*, *481*, 126555. https://doi.org/10.1016/j.optcom.2020.126555

Habib, A., Rashed, A. N. Z., El-Hageen, H. M., & Alatwi, A. M. (2021). Extremely sensitive photonic crystal fiber–based cancer cell detector in the terahertz regime. *Plasmonics*, *16*(4), 1–10. https://doi.org/10.1007/s11468-021-01409-6

Hossain, M. S., Kamruzzaman, M. M., Sen, S., & Azad, M. M. (2021). *Hexahedron core with sensor based photonic crystal fiber: An approach of design and performance analysis* (p. 100426). Sensing and Bio-Sensing Research.

Iovanna, P., Bigongiari, A., Cavaliere, F., Bianchi, A., Testa, F., Marconi, S., et al. (2021). Optical components for transport network enabling the path to 6G. *Journal of Lightwave Technology*, *40*(2), 527–537. https://doi.org/10.1109/jlt.2021.3117122

Islam, M. A., Islam, M. R., Al Naser, A. M., Anzum, F., & Jaba, F. Z. (2021). Square structured photonic crystal fiber based THz sensor design for human body protein detection. *Journal of Computational Electronics*, *20*(1), 377–386. https://doi.org/10.1007/s10825-020-01606-2

Islam, M. I., Khatun, M., & Ahmed, K. (2017). Ultra-high negative dispersion compensating square lattice based single mode photonic crystal fiber with high nonlinearity. *Optical Review*, *24*(2), 147–155. https://doi.org/10.1007/s10043-017-0308-0

Kalantari, M., Karimkhani, A., & Saghaei, H. (2018). Ultra-wide mid-IR supercontinuum generation in As2S3 photonic crystal fiber by rods filling technique. *Optik*, *158*, 142–151. https://doi.org/10.1016/j.ijleo.2017.12.014

Leon, M. J. B. M., Abedin, S., & Kabir, M. A. (2021). A photonic crystal fiber for liquid sensing application with high sensitivity, birefringence and low confinement loss. *Sensors International*, *2*, 100061. https://doi.org/10.1016/j.sintl.2020.100061

Li, J., Zhao, F., & Hui, Z. (2019). Mid-infrared supercontinuum generation in dispersion-engineered highly nonlinear chalcogenide photonic crystal fiber. *Modern Physics Letters B*, *33*(19), 1950211. https://doi.org/10.1142/s0217984919502117

Liao, J., Huang, T., Xiong, Z., Kuang, F., & Xie, Y. (2017). Design and analysis of an ultrahigh birefringent nonlinear spiral photonic crystal fiber with large negative flattened dispersion. *Optik*, *135*, 42–49. https://doi.org/10.1016/j.ijleo.2017.01.054

Maidi, A. M. I., Yakasai, I., Abas, P. E., Nauman, M. M., Apong, R. A., Kaijage, S., & Begum, F. (2021). Design and simulation of photonic crystal fiber for liquid sensing. In *Photonics* (Vol. 8, p. 16). Multidisciplinary Digital Publishing Institute.

Medjouri, A., Abed, D., & Becer, Z. (2019). Numerical investigation of a broadband coherent supercontinuum generation in Ga8Sb32S60 chalcogenide photonic crystal fiber with all-normal dispersion. *Opto-Electronics Review*, *27*, 1–9. https://doi.org/10.1016/j.opelre.2019.01.003

1944799x, 2023, 9, Downloaded from https://agupubs.onlinelibrary.wiley.com/doi/10.1029/2023RS007690 by Cochrane France, Wiley Online Library on [13/10/2023]. See the Terms and Conditions (https://onlinelibrary.wiley.com/terms-and-conditions) on Wiley Online Library for rules of use; OA articles are governed by the applicable Creative Commons License

Michaeli, L., & Bahabad, A. (2018). Genetic algorithm driven spectral shaping of supercontinuum radiation in a photonic crystal fiber. *Journal of Optics*, *20*(5), 055501. https://doi.org/10.1088/2040-8986/aab59c

Moon, S. R., Kim, E. S., Sung, M., Rha, H. Y., Lee, E. S., Lee, I. M., et al. (2021). 6G indoor network enabled by photonics-and electronics-based sub-THz technology. *Journal of Lightwave Technology*, *40*(2), 499–510. https://doi.org/10.1109/jlt.2021.3113898

Paul, B. K., Ahmed, F., Moctader, M. G., Ahmed, K., & Vigneswaran, D. (2018). Silicon Nano crystal filled photonic crystal fiber for high nonlinearity. *Optical Materials*, *84*, 545–549. https://doi.org/10.1016/j.optmat.2018.07.054

Paul, B. K., Khalek, M. A., Chakma, S., & Ahmed, K. (2018). Chalcogenide embedded quasi photonic crystal fiber for nonlinear optical applications. *Ceramics International*, *44*(15), 18955–18959. https://doi.org/10.1016/j.ceramint.2018.07.134

Paul, B. K., Rajesh, E., Asaduzzaman, S., Islam, M. S., Ahmed, K., Amiri, I. S., & Zakaria, R. (2018). Design and analysis of slotted core photonic crystal fiber for gas sensing application. *Results in Physics*, *11*, 643–650. https://doi.org/10.1016/j.rinp.2018.10.004

Qu, Y., Yuan, J., Qiu, S., Zhou, X., Li, F., Yan, B., et al. (2021). A novel gold film-coated v-shape dual-core photonic crystal fiber polarization beam splitter covering the E+ S+ C+ L+ U band. *Sensors*, *21*(2), 496. https://doi.org/10.3390/s21020496

Raddo, T. R., Rommel, S., Cimoli, B., Vagionas, C., Perez-Galacho, D., Pikasis, E., et al. (2021). Transition technologies towards 6G networks. *EURASIP Journal on Wireless Communications and Networking*, *2021*(1), 1–22. https://doi.org/10.1186/s13638-021-01973-9

Rajesh, A., Chandru, S., & Robinson, S. (2021). Investigation of defective hybrid cladding with silicon nanocrystal PCF for supercontinuum generation. *Laser Physics*, *31*(8), 126206. https://doi.org/10.1088/1555-6611/ac32da

Rao, M. S., & Singh, V. (2018). Dispersion and nonlinear properties of elliptical air hole photonic crystal fiber. *Current Optics and Photonics*, *2*(6), 525–531.

Rifat, A. A., Ahmed, K., Asaduzzaman, S., Paul, B. K., & Ahmed, R. (2019). Development of photonic crystal fiber-based gas/chemical sensors. In *Computational photonic sensors* (pp. 287–317). Springer.

Saghaei, H. (2017). Supercontinuum source for dense wavelength division multiplexing in square photonic crystal fiber via fluidic infiltration approach. *Radioengineering*, *26*(1), 16–22. https://doi.org/10.13164/re.2017.0016

Salgueiro, J. R., & Ferrando, A. (2018). Spatial solitons in nonlinear photonic crystal fibers. In *Nonlinear systems* (Vol. 2, pp. 139–171). Springer.

Seifouri, M., & Alizadeh, M. R. (2018). Supercontinuum generation in a highly nonlinear chalcogenide/MgF2 hybrid photonic crystal fiber. *International Journal of Ophthalmic Practice*, *12*(1), 69–78. https://doi.org/10.29252/ijop.12.1.69

Sharma, M., & Konar, S. (2016). Broadband supercontinuum generation in lead-silicate photonic crystal fibers employing optical pulses of 50W peak power. *Optics Communications*, *380*, 310–319. https://doi.org/10.1016/j.optcom.2016.06.027

She, Y. L., Zhang, W. T., Tu, S., & Liang, G. (2021). Large mode area single mode photonic crystal fiber with ultra-low bending loss. *Optik*, *229*, 165556. https://doi.org/10.1016/j.ijleo.2020.165556

Singh Saini, T., Kumar, A., & Sinha, R. K. (2015). Broadband mid-infrared supercontinuum spectra spanning 2–15 μm using As2Se3 chalcogenide glass triangular-core graded-index photonic crystal fiber. *Journal of Lightwave Technology*, *33*(18), 3914–3920. https://doi.org/10.1109/jlt.2015.2418993

Sung, M., Moon, S. R., Kim, E. S., Cho, S., Lee, J. K., Cho, S. H., et al. (2021). Design considerations of photonic THz communications for 6G networks. *IEEE Wireless Communications*, *28*(5), 185–191. https://doi.org/10.1109/mwc.001.2100002

Vyas, A. K. (2021). Multiple rings based photonic crystal fiber for terahertz application. *Optik*, *231*, 166424. https://doi.org/10.1016/j.ijleo.2021.166424

Wang, W., Sun, C., Wang, N., & Jia, H. (2020). A design of nested photonic crystal fiber with low nonlinear and flat dispersion supporting 30+ 50 OAM modes. *Optics Communications*, *471*, 125823. https://doi.org/10.1016/j.optcom.2020.125823

Xiong, D., Bai, Y., Zuo, D., & Wang, X. (2021). High-resolution continuous-wave coherent anti-Stokes Raman spectroscopy in a CO2-filled hollow-core photonic crystal fiber. *Journal of Raman Spectroscopy*, *52*(4), 857–864. https://doi.org/10.1002/jrs.6076

Yang, T., Zhang, L., Shi, Y., Liu, S., & Dong, Y. (2021). A highly birefringent photonic crystal fiber for terahertz spectroscopic chemical sensing. *Sensors*, *21*(5), 1799. https://doi.org/10.3390/s21051799

Yu, B., & Rui, H. (2019). A simple design of highly birefringent and nonlinear photonic crystal fiber with ultra-flattened dispersion. *Optical and Quantum Electronics*, *51*(11), 1–13. https://doi.org/10.1007/s11082-019-2091-6

Zheng, G. M. (2021). Mid-infrared broadband polarization beam splitter based on GaS photonic crystal fiber with high extinction ratio. *Optik*, *241*, 166971. https://doi.org/10.1016/j.ijleo.2021.166971

Erratum

In the originally published version of this article, the third author's affiliation should have been "School of Electronics Engineering, Vellore Institute of Technology, Vellore, India" rather than "VIT-AP University, Amarvati, India." The affiliation has been corrected, and this may be considered the authoritative version of record.

19447799x, 2023, 9, Downloaded from https://agupubs.onlinelibrary.wiley.com/doi/10.1029/2023RS007690 by Cochrane France, Wiley Online Library on [13/10/2023]. See the Terms and Conditions (https://onlinelibrary.wiley.com/terms-and-conditions) on Wiley Online Library for rules of use; OA articles are governed by the applicable Creative Commons License